J Nanopart Res
DOI 10.1007/s11051-008-9499-4

Exposure to nanoscale particles and fibers during machining of hybrid advanced composites containing carbon nanotubes

Dhimiter Bello · Brian L. Wardle · Namiko Yamamoto · Roberto Guzman deVilloria · Enrique J. Garcia · Anastasios J. Hart · Kwangseog Ahn · Michael J. Ellenbecker · Marilyn Hallock

Received: 26 January 2008 / Accepted: 22 August 2008

Abstract This study investigated airborne exposures to nanoscale particles and fibers generated during dry and wet abrasive machining of two three-phase advanced composite systems containing carbon nanotubes (CNTs), micron-diameter continuous fibers (carbon or alumina), and thermoset polymer matrices. Exposures were evaluated with a suite of complementary instruments, including real-time particle number concentration and size distribution (0.005–20 μm), electron microscopy, and integrated sampling for fibers and respirable particulate at the source and breathing zone of the operator. Wet cutting, the usual procedure for such composites, did not produce exposures significantly different than background whereas dry cutting, without any emissions controls, provided a worst-case exposure and this article focuses here. Overall particle release levels, peaks in the size distribution of the particles, and surface area of released particles (including size distribution) were not significantly different for composites with and without CNTs. The majority of released particle surface area originated from the respirable (1–10 μm) fraction, whereas the nano fraction contributed $\sim$10% of the surface area. CNTs, either individual or in bundles, were not observed in extensive electron microscopy of collected samples. The mean number concentration of peaks for dry cutting was composite dependent and varied over an order of magnitude with highest values for thicker laminates at the source being $>1 \times 10^6$ particles cm^{-3}. Concentration of respirable fibers for dry cutting at the source ranged from 2 to 4 fibers cm^{-3} depending on the composite type. Further investigation is required and underway to determine the effects of various exposure determinants, such as specimen and tool geometry, on particle release and effectiveness of controls.

Keywords Nanoparticle · Nanocomposite · Fiber · CNTs · Airborne exposures · Occupational health · Nanotechnology · EHS

D. Bello (✉) · K. Ahn · M. J. Ellenbecker
Department of Work Environment, University of Massachusetts Lowell, Lowell, MA 01854, USA
e-mail: dhimiter_bello@uml.edu

B. L. Wardle · N. Yamamoto · R. Guzman deVilloria · E. J. Garcia · A. J. Hart
Technology Laboratory for Advanced Materials and Structures, Department of Aeronautics & Astronautics, Massachusetts Institute of Technology, Cambridge, MA 02139, USA

M. Hallock
Environmental Health & Safety, Massachusetts Institute of Technology, Cambridge, MA 02139, USA

Introduction

New structural composite concepts harnessing the attractive properties of carbon nanotubes (CNTs) are

being intensely researched around the world (Ajayan and Tour 2007; Coleman et al. 2006; Lavine 2006; Schulte and Windle 2007; Thostenson et al. 2005). Nanocomposites (nanostructures in a matrix) (Ajayan et al. 2003) and hybrid composites (nanostructures in the matrix of a traditional fiber composite) exist (Garcia et al. 2008a, b). Carbon nanotubes (CNTs) are the most prominent nanostructure, and polymers (both thermoset and thermoplastic) are a common matrix to combine with CNTs. Typical processing of an advanced composite involves temperature and pressure/vacuum application to cure the matrix in the composite. Subsequent processing of the advanced composite involves drilling and cutting as with metallic structures, except that abrasive processes (e.g., diamond-grit cutting wheels) are used rather than conventional cutting tools.

A significant concern related to processing of the nanocomposites and hybrid composites is exposure to nanoscale particles due to concerns over nanoparticle toxicity. The possible release of CNTs from CNT-containing composites, in addition to other nanoparticles or respirable fibers, during their processing such as cutting, machining, etc. is of special interest from an occupational health and hygiene perspective. Limited animal studies relate CNTs and other nanoscale particles to possible adverse health effects, such as pulmonary inflammation, oxidative stress, onset of early interstitial fibrosis, and granulomas (Donaldson et al. 2006; Lam et al. 2004, 2006; Shvedova et al. 2005). A recent study by Poland et al. (2008) in which long CNTs were shown to possess asbestos-like pathogenicity has raised great concerns about the possibility of such exposure to nanomaterials. Similar concerns exist about potential exposures to other nanoscale carbonaceous particles, such as carbon black, which have been shown to cause oxidative damage in biologically relevant media such as human blood serum (Barlow et al. 2005a, b; Foucaud et al. 2007; Rogers et al. 2008).

The main objective of this study was to characterize airborne exposures generated during the processing of two types of hybrid (CNTs, advanced fibers, and polymer matrix) composites in a research laboratory setting. Of particular interest is identifying differences in baseline (no CNT) and CNT-containing composites as it relates to overall exposure characteristics, particularly the release of individual or bundles of CNTs. The emphasis is on exposures to nanoscale particles (especially identification of any CNTs) and respirable fibers at the source and the breathing zone of operator, and not exposure determinants or controls. A prior paper has reported on nanoscale particle exposure during CNT synthesis and handling (Bello et al. 2008). The CNTs used in the previous study, and used to fabricate the hybrid composites in this study, are aligned, continuous, and small diameter (10–20 nm avg.), multi-walled structures grown from a base-growth CVD mechanism leading to CNT concentration of 10–100 billion CNTs per cm^2 of substrate growth area.

Methods

Fabrication of hybrid CNT composites

Two different types of hybrid CNT composites (see Fig. 1) were fabricated to investigate particle emission during processing. The first was a graphite-epoxy prepreg[1] system (aligned carbon fibers with an epoxy resin arranged in a layered laminate configuration) with aligned CNTs placed at the center ply interface (Garcia et al. 2008b), termed here 'CNT–carbon' composite for simplicity. The second CNT–hybrid composite is a woven alumina (Al_2O_3) fiber cloth with aligned CNTs grown on the surface of the fibers, impregnated with an epoxy (Garcia et al. 2008a), termed herein 'CNT–alumina' composite. Samples without CNTs were also fabricated (baseline composites) for comparison to the CNT–hybrid composites.

Both CNT-containing composites employ capillarity-driven wetting (Garcia et al. 2007) to fully combine the CNTs and the polymer epoxies, i.e., the CNTs are surrounded and in contact with the polymer. Fabrication of the two CNT-containing composites was as follows. The CNT–carbon fabrication begins by growing vertically aligned continuous multiwalled CNTs (8 nm average diameter, 100–150 μm long) on a silicon wafer substrate coated with a Fe/Al_2O_3 catalyst layer using atmospheric pressure CVD in C_2H_4/H_2 at 750 °C (Hart and Slocum 2006). Next, the CNT forests were transplanted to an AS4/8552 (Hexcel Corp., Duxford, UK), carbon fiber (7 μm in diameter), and epoxy prepreg

[1] Carbon fibers are pre-impregnated with a partially cured thermosetting polymer to form the raw 'prepreg' layer that is stacked in layers and cured to form a laminate.

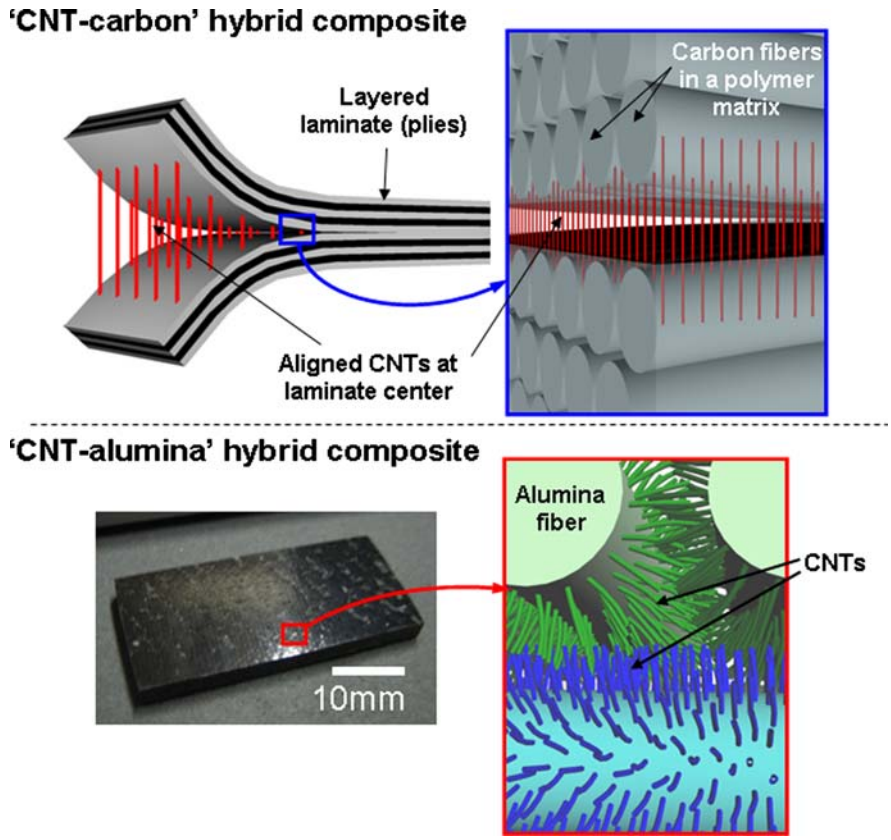

Fig. 1 Illustration of the two CNT–hybrid composite architectures investigated: 'CNT–carbon' nanostitched prepreg and 'CNT–alumina' fuzzy fiber advanced composites

ply. Prepreg plies are stacked with a suitable combination of fiber directions, and are cured to form aerospace structural composites that are strong and light. The aligned CNT film is transplanted (Garcia et al. 2008b) to the tacky prepreg surface, using the sticky uncured epoxy to fix the CNT film to the prepreg. Other prepreg layers were added, always with the carbon fibers aligned in the same direction, to form a laminate with 24 plies, 12 plies of $\sim$130 microns thick on each side above and below the CNT film. The 24-ply CNT–carbon composites were $\sim$2.9-mm thick. The prepreg laminate was cured under heat (180 °C) and pressure (7 bar or 100 psi) following standard procedures for this material system. The CNT–carbon system has $\sim$0.05% CNTs by volume of the laminate ($\sim 50 \times 10^9$ CNTs cm^{-2} of laminate area) giving $\sim 0.1 \times 10^{12}$ CNTs cm^{-3} in the CNT–carbon composite.

In order to fabricate the CNT–alumina composite, a woven Al_2O_3 fiber (11-μm diameter) cloth was coated with Fe catalyst by dip-coating in a solution of $Fe(NO_3)_3 \cdot 9H_2O$ dissolved in 2-propanol. Instead of the Si wafer, alumina fiber cloth is used as the growth substrate. After dip-coating with an iron–salt catalyst, continuous multiwalled CNTs were grown (17 nm average diameter and $\sim$50-μm length) on the fiber surfaces using the same CVD conditions as for CNTs on the wafer substrates. Epoxy was added to this CNT-grown cloth ply, and plies stacked together and then cured to a laminate at $\sim$50 °C and pressure ($\sim$200 kPa). Thus, CNTs in the CNT–alumina composites are distributed throughout the CNT–alumina hybrid composite laminate. The thickness of tested CNT–alumina composites varied from 0.6 (1 ply) to 2.9 mm (4 plies). The CNT volume fraction in the CNT–alumina composites varied from 0.5 to 4.5% depending on the sample, giving $\sim 1 \times 10^{12}$ CNTs cm^{-3} in the CNT–alumina composites. Base–alumina composites of 1–4 plies without CNTs were also fabricated.

Machining of hybrid CNT composites

Samples were machined using two different methods: band-saw and a rotary cutting wheel. The band-saw blade is a diamond-grit (220 grit, $\sim$60 μm) abrasive

specific for composite machining. The band-saw blade width is 1.65 mm and was used at a blade speed of 20 m s^{-1} with the rate of advance of the composites being $\sim$0.2–0.4 cm s^{-1}. Composite cutting wheels use the same kind of abrasive surface, but with water to flush dust particles during machining. The cutting wheel blade width is 1.60 mm and was used at a blade speed of 15 m/s with the rate of advance of the composites being $\sim$0.4 cm s^{-1}. The cutting wheel was covered with guards on all sides, which helped to reduce aerosol emissions. Thus, in the following, we call the former as dry cutting, and the latter as wet cutting. Vacuum and other emission control measures are typically used in dry cutting of such composites, but no such measures were employed here so that the study could focus on exposures under a worst-case scenario. The size of the samples before cutting was in the range of $\sim 10 \times 50$ mm (width $\times$ length). Sample thickness (Table 1) varied with the composite type depending on the number of plies and presence of CNTs. The carbon–fiber composites were cut perpendicular to the direction of the aligned carbon fibers; since the woven alumina cloth has fibers in both directions, the direction of the cut is not important. Note that composites have preferred (wet vs. dry) machining procedures (e.g., base carbon is typically wet cut), but both were used here for purposes of exposure comparison.

Laboratory setting

A schematic layout of the research laboratory where this study took place is shown in Fig. 2A. The lab was located in the basement of the building and was supplied with general mechanical ventilation of one room exchange rate per hour. It had no direct air exchange with the outside environment (such as through windows or window-positioned air conditioning units). No activities which could generate nanoscale particles and interfere with the study took place during any of the test sessions in the lab. Additionally, none of the present equipment in the lab, apart from the ones that were part of the study, was running. No other activities or processes (compressors, pumps, diesel, or propane combustion engines, photocopiers, printers, floor cleaning equipment, etc.) that could generate significant amounts of nanoscale particles and interfere with the study were present. The main door next to the band-saw stage was kept closed as is normal. The door was opened intentionally between tests to shorten the time needed to return airborne exposures to background levels prior to subsequent tests. Typical metrological parameters during the monitoring periods were: temperature 20–22 °C, relative humidity 39–42%, and CO_2 concentration 390–456 ppm.

Exposure characterization

The processes were monitored on three different occasions over the course of 1 year (session one on July 31, 2007; session two on January 16, 2008; session three on June 12, 2008). Since one cut took on average 5–15 s to complete, up to four cuts were performed on each composite to improve reliability of the data. The whole cycle of 4–5 cuts lasted $\sim$1–3 min. A tiered approach was adopted for collection of data for this study to accommodate the complexity of logistic and technical issues, including: sample destruction by the tests and the limited number of cuts per specimen (3–5); the availability of the novel hybrid composites; acquisition of and availability of a suite of expensive instrumentation at the time of sampling; and time intensive imaging and data analyses of collected samples. In this tiered approach, each subsequent test utilized the findings of prior tests to improve the sampling strategy. Therefore, some changes in the protocol and the nature of data did exist between sessions. The primary focus of monitoring became dry cutting since two preliminary tests (summary results presented here) identified it as a significant particle exposure generating process. The last session was the most comprehensive.

The sampling strategy focuses on dry cutting using the band saw and included: characterization of exposures during dry cutting at two different angles: 45° (session three, Fig. 2B—location 1, source emission and breathing zone data) and 135° (sessions one and two, Fig. 2B—location 2, source emission) using continuous, real time monitoring of particle number concentration and size distribution from 5.6 nm to 20 μm, integrated area and breathing zone samples for respirable fibers, respirable dust, and subsequent electron microscopy analysis. Sampler inlets for source monitoring were positioned 10 cm away from the point source; sampler arrangements in relation to the band saw and the operator are shown in Fig. 2B. The operator was within arms distance from the point

Table 1 Summary of airborne exposures *at the source* (location 1 in Fig. 2B) as a function of composite parameters during dry cutting[a]

Composite	Laminate specifications		AM (SEM) of total number concentration (# cm^{-3})		AM surface area (μm^2 cm^{-3}) by size range (its fraction of the total surface area)						
	No. plies	CNT fraction (# cm^{-3})	FMPS	APS	$d_p \leq 0.1$ μm	$0.1 < d_p \leq 1.0$ μm	$1 < d_p \leq 10$ μm	$10 < d_p \leq 20$ μm	$\sum$	RF (F cm^{-3})	AM PM_{10} dust (mg m^{-3})
Background	–	–	4.82E + 3 (0.63E + 4)	11.4 (0.08)	286 (0.26)	340 (0.29)	642 (0.44)	10 (0.00)	1,279 (1.0)	–	0.013
Wet cutting (with broken guard) of base–carbon	24	–	9.4E + 4 (0.28E + 4)	47.6 (2.0)	12,580 (0.11)	99,373 (0.85)	4,077 (0.04)	68 (0.00)	116,098 (1.0)	–	0.054
Dry cutting											
Base–alumina	4	–	1.48E + 5 (3.7E + 4)	135.2 (4.8)	6,367 (0.10)	4,429 (0.06)	65,551 (0.83)	863 (0.01)	77,211 (1.0)	1.6	1.19
CNT–alumina	4	2.0 E + 12	0.38E + 5 (0.13E + 4)	285.3 (19.1)	1,118 (0.01)	17,046 (0.14)	214,506 (0.84)	2,281 (0.01)	234,950 (1.0)	1.6	2.11
Base–carbon	24	–	2.83E + 5 (9.5E + 4)	1003.8 (33.5)	6,914 (0.02)	35,056 (0.09)	411,140 (0.89)	3,944 (0.01)	457,053 (1.0)	3.8	5.61
CNT–carbon	24	1.5 E + 11	2.94E + 5 (1.7E + 4)	867.1 (52.2)	7,809 (0.04)	40,898 (0.25)	339,971 (0.71)	4,386 (0.01)	393,063 (1.0)	–[b]	8.38

d_p, Aerodynamic diameter; AM, arithmetic mean; SEM, standard error of mean; FMPS, fast mobility particle sizer instrument; APS, aerodynamic particle sizer instrument; $\sum$, sum; RF, respirable fibers (length > 5–20 μm, aspect ratio >3) measured in fibers per cubic centimeter (F cm^{-3}); PM_{10}, particulate matter < 10 μm (equivalent to respirable dust) measured by Dust Track, background corrected. All laminates 2.9-mm thick

[a] In five prior tests exposures during wet cutting were statistically not different from background and no fiber sampling was conducted during this last session. Reported source exposures for wet cutting are from the machine with a broken guard

[b] Pump failure, unreliable measurement

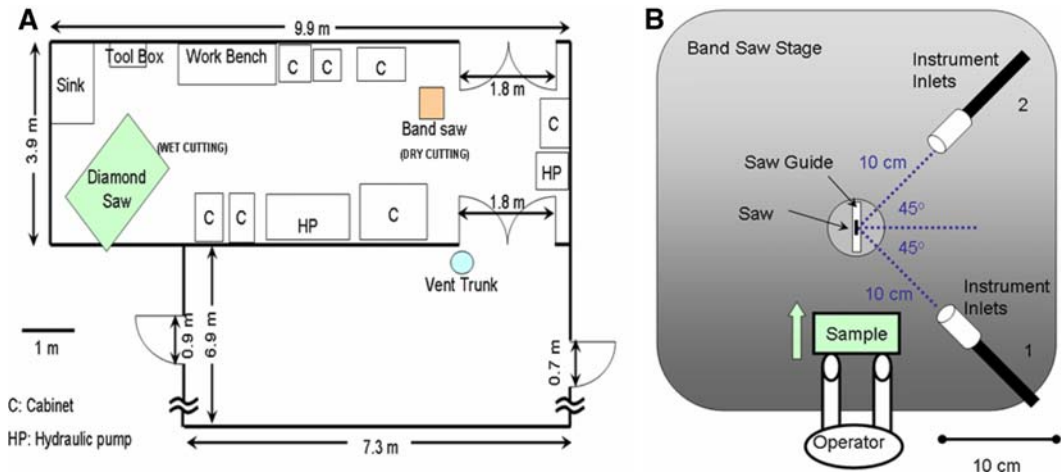

Fig. 2 (**A**) Layout of the research lab. Band saw was used for dry cutting, whereas diamond saw for wet cutting. (**B**) Layout of the band-saw stage indicating the two positions monitored for source emission in relation to the operator. Instrument inlets were on top of the band-saw stage

source perpendicular to the band-saw plane. The band rotation produced a downward (toward the floor) direction of particle trajectory. Wet cutting was monitored near the breathing zone of the operator (90° angle from the plane of the rotary wheel) due to concerns over instrument damage from high water aerosol concentrations and limited access. The breathing zone for wet cutting was also at arms length distance from the point source. The research team wore N100 respirators, gloves, and lab coats during all monitoring sessions and limited the access of other personnel in the lab during all tests until exposures had returned to background level.

Instrumentation and analysis

Measurements of airborne particles (>5.6 nm–20 μm) were accomplished using a suite of complementary instruments, including:

- Two real-time particle sizers (FMPS Model 3091 and APS 3321, both from TSI Inc., St. Paul, MN, USA). The FMPS measures the number concentration of aerosol particles in the range from 5.6 to 560 nm, for a total of 32 channels based on particle mobility diameter, with a response time of 1 s, and continuous monitoring for up to 12 h. The FMPS operates at 10 L/min. The measurement range of the FMPS is particle size dependent: its minimum varies from ~ 100 particles cm^{-3} at 10 nm to ~ 10 particles cm^{-3} at 100 nm, whereas its maximum varies from $\sim 5 \times 10^5$ to 5×10^6 particles cm^{-3}, respectively. The APS measures number concentration of particles in the range of 0.5–20 μm in 52 channels based on their aerodynamic diameter and has a similar response time of 1 s, and 18 h of continuous operation. Its optimum concentration range is 0.001–1,000 particle cm^{-3}. The APS operates at a sampling flow rate of 1 L/min (total flow rate 5 L/min). The APS became available only on the last monitoring session (location 2, Fig. 2B).
- A condensation particle counter (TSI CPC 3007), which measures the total particle number concentration in the range of 10 nm to ~ 1 μm particles cm^{-3}, but not size distribution. The CPC 3007 has a lower limit of detection of 1 particle cm^{-3} and an upper linear range of 10^5 particles cm^{-3} and operates at an inlet sampling flow rate of 0.7 L min^{-1}.
- A thermophoretic precipitator (TP, Fraunhofer Institute of Toxicology, Germany) and an electrostatic precipitator (ESP, courtesy of Dr. A. Miller, Spokane Laboratory, NIOSH, WV). These instruments use a thermal gradient and electrical discharge, respectively, to collect particles on a TEM Cu grid for electron microscopy characterization. Both instruments were used side-by-side in most cases. Two TEM grids were collected and analyzed for each process. The reasons for this conservative approach are numerous, including the prototype nature of the ESP sampler, possible unexpected instrument failures, uncertainties/

differences in collection efficiencies and possible damage, contamination, or loss of the TEM grids in the field or laboratory. The sampling time for both instruments was matched to the duration of the process, often 3–5 min. The TP was operated at a probe temperature of 140 °C and tip temperature of 42 °C. The TEM grids (Electron Microscopy Sciences, Hatfield, PA) were 200-mesh Cu with a silicon monoxide (ESP) or C film (TP).

– Sampling for respirable fibers (length > 5–20 μm and aspect ratio >3) was conducted as per NIOSH Method 7400 with a commercially available asbestos sampling cassette (Millipore Inc., Bedford, MA; 25-mm, 0.45 μm pore size mixed-cellulose ester filter equipped with an electrically conductive 50-mm extension cowl and operated at 2 L min^{-1}). Samples were collected at the source (Fig. 2B, location 1, for each of the four processes; location 2, base–alumina and CNT–alumina) and one integrated sample over the whole dry cutting process at the breathing zone for both locations. Additionally, one integrated breathing zone respirable dust sample was collected for location 1 with a high flow GK 2.69 respirable cyclone (BGI Inc., Waltham, MA) operated at 4.2 L min^{-1}. Personal sampling pumps (Gilian, Wayne, NJ) were calibrated before and after sampling with a DryCal DC-Lite primary flowmeter (Bios International Co., Pompton Plains, NJ).
– A factory calibrated TSI Dust Trak™ was also used to measure in real time total particle mass concentration. The Dust Trak was operated with tubing attached to the 10 μm inlet and was used as a surrogate measure of airborne aerosol mass concentration.

Instrument inlets were bundled together using conductive tubing at the minimum physical separation distance and positioned 10 cm away from the point emission source at the 45 and 135° angles and in the breathing zone of operator.

Analysis for respirable fibers was conducted using NIOSH Method 7400 by PCM (Phase Contrast Microscopy). One of the breathing zone respirable fiber filters was also analyzed by SEM (JEOL JSM-7401F), whereas the TEM grids were analyzed by TEM (Philips EM 400T) for particle size and morphology. One half of the respirable fiber filter was coated with nano gold to improve its conductivity and the area thoroughly scanned primarily to get a better understanding of the morphology, elemental composition, and possibly the origin of respirable fibers. Elemental analysis for particles of interest was obtained with the integrated energy dispersive spectroscopy (EDS) detectors (EDAX) present on both instruments. Twenty-one TEM grids (~3-mm diameter, surface area 7.1 μm^2) were collected in all, 15 of which were analyzed by TEM. The glass slides of the two breathing zone fiber filters were also scanned with an Olympus FV300 Confocal Fluorescence Microscope to acquire digital images of microscopic particles. Statistical analysis of the data from real time monitoring instruments (FMPS, APS, CPC, Dust Trak) was conducted in SPSS v15 (Chicago, IL). Differences in exposure levels between processes were evaluated with ANOVA.

Results

Total particle number concentration

Dry cutting

The total number concentration at the source as measured by FMPS, APS, and CPC 3007 for location 1 (Fig. 2B) is presented in Fig. 3A (FMPS) and Fig. 3B (APS), and for location 2 (Fig. 2B) in Fig. 4A (FMPS) and Fig. 4B (CPC 3007, no APS was available during this monitoring session). The CPC 3007 data for location 1 is omitted to avoid redundancy.

Dry cutting of composites generated statistically significant quantities of nanoscale and fine particles as compared to background ($p < 0.05$), regardless of the composite type (CNT–carbon, CNT–alumina, and their respective base composites), as expected. The background concentration of particles in the 5.6–560 nm range as measured by FMPS was ~4,000 particles cm^{-3} (Figs. 3A and 4A), and increased sharply during cutting of different composites. Exposures at the source were similar for both locations, although higher concentrations were recorded for carbon composites at location 2. CNT–carbon and base–carbon composites generated a maximum of 2–5 × 10^6 particles cm^{-3} at location 2 (Fig. 4A) and 5–7 × 10^5 particles cm^{-3} at location 1. Differences within a factor of two and without any particular trend were

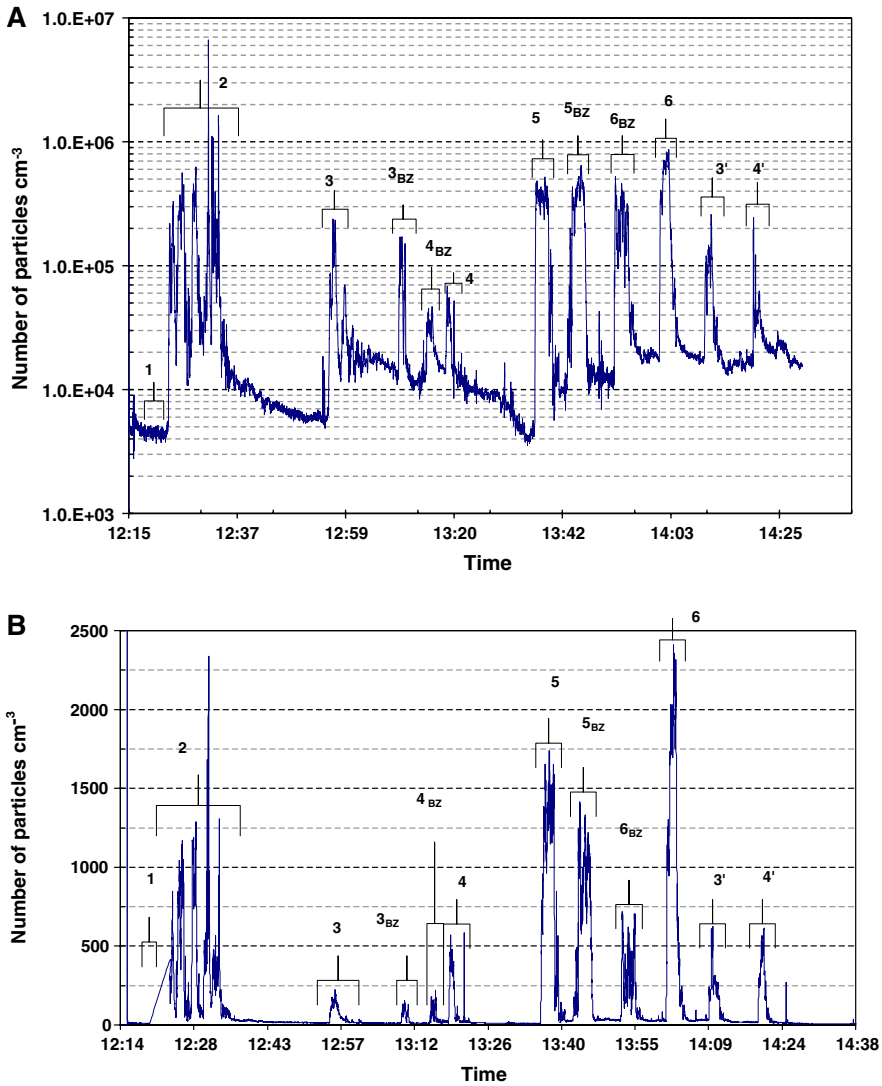

Fig. 3 Total particle number concentration for dry cutting over the combined range 0.005–20 μm as measured by FMPS (**A**; 5.6–560 nm) and APS (**B**; <0.5–20 μm) at the source and breathing zone of the operator for location 1 in Fig. 2B. The CPC 3007 data (omitted) paralleled FMPS and APS data, with maxima in the range of 0.5–2.0E + 5 particles cm^{-3}. Legend: BZ—Breathing zone measurements for the corresponding process; 1. Background; 2. Trimming edges of various composites; All others represent dry cutting of: 3. base alumina, four plies, three cuts; 3′-same as 3; 4. CNT–alumina, four plies, three cuts; 4′-same as 4; 5. base carbon; 24 plies, three cuts; 6. CNT–carbon, 24 plies, three cuts

seen for carbon composites. In contrast, the 4-ply base–alumina composites generated significantly higher (3–10×) particulate number concentration compared to the 1–4 ply CNT–alumina composites at both locations. Equivalent thickness alumina composite exposures are discussed subsequently. The maximum total particle number concentrations (TPNC) for base–alumina were $\sim 2 \times 10^5$ particles cm^{-3}, whereas for CNT–alumina ~ 2–5×10^4 particles cm^{-3}. The maximum total particle number (TPN) as measured by APS (0.5–20 μm, Fig. 3B) ranged from a low of 15 (background) to a maximum of 2,400 particles cm^{-3} for CNT–carbon composites. Mean TPNC values ranged from 11 (background) to 1,004 (base–carbon) particles cm^{-3}. The total particle number in the 10–1,000 nm (Fig. 4B) increased from a background value of ~ 3–4×10^3 particles cm^{-3} to >100,000 during dry cutting and paralleled very well the FMPS data during all measurements. The difference in the TPNC between base alumina vs. base–carbon and CNT–carbon composites was smaller than for FMPS data. This is likely caused by saturation of the CPC detector, since the total particle number concentration is notably higher than the upper instrument linear range of 10^5 particles cm^{-3}. For the alumina composites, particle emission would logically scale with the thickness of the laminate and therefore the 1-ply CNT–alumina would generate fewer particles than the 4-ply alumina composite, as observed.

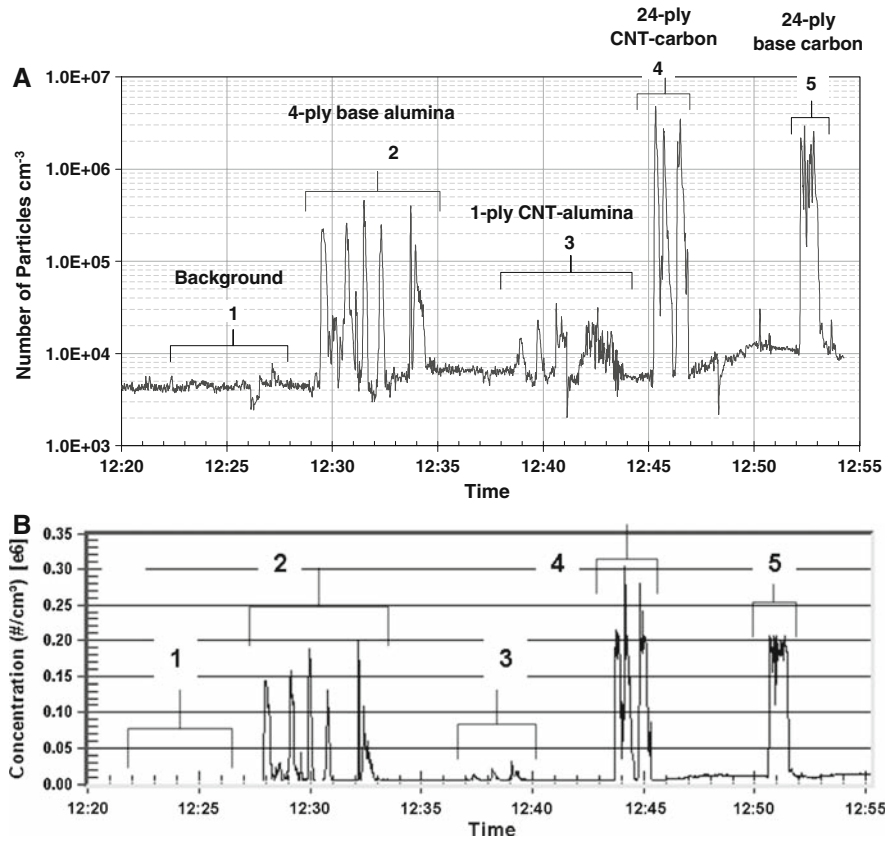

Fig. 4 Total particle number concentration for dry cutting over the combined range of 0.005–1 μm as measured by FMPS (**A**; 5.6–560 nm) and CPC 3007 (**B**; 10 nm–1 μm) at the source for location 2 in Fig. 2B. Legend: 2. Five cuts; 3. four cuts; 4. four cuts; 5. five cuts

This hypothesis was tested with a separate set of composites (Jan 16, 2008 testing, location 2) with directly comparable specifications including thickness. Here, 1-, 2-, and 3-ply base–alumina composites and 1- and 2-ply CNT–alumina composites were dry cut an average of four times each. The total particle number concentration as measured by FMPS (Figure omitted) varied between 0.9–1.4 $\times$ 10^5 particles cm^{-3} for base–alumina and 3–6 $\times$ 10^4 particles cm^{-3} for CNT–alumina composites. The TPNC was of the same order of magnitude as shown in Figs. 3A and 4A, and dependent on both the number of plies and type of composite (CNTs or no CNTs).

Mean breathing zone TPNC (for location 1) were 2–5 times lower than source measurements (Tables 1 and 2), except for the FMPS data of the base–carbon composites, which were slightly higher than the source.

Wet cutting

Wet cutting of base–carbon and CNT–carbon composites in all, but the June 12th, 2008 (third) tests resulted in no statistically significant TPNC increases above background ($p > 0.05$; data omitted). The June 12th measurements were in sharp contrast to prior observations (Fig. 5A). In these latest tests (Fig. 5B, C), mean TPNC for FMPS and APS was 9.4E + 4 and 76.8 (range of tests means 65.0–96.7) particles cm^{-3}, respectively, which is significantly higher than background values of 4.82E + 3 and 11.4 particles cm^{-3}. Maximum values were 5.5E + 5 and 380.7 particles cm^{-3}, respectively. Aerosol emissions during the last (June 12th) round of tests were related visually to extensive damages of the protective guard around the rotary wheel. The FMPS TPNC remained elevated throughout multiple cuts, whereas APS TPNC paralleled the wet cutting cycle as seen in the clearly defined cluster of tests.

Particle size distribution

Particle size distribution in the combined range of 5.6 nm–20 μm for various processes of Fig. 3 (test location 1 in Fig. 2B) is shown in Fig. 6. Size distributions were commonly polydisperse with maxima occurring at 12, 20, 230 ± 20 nm and 1 ±

0.1 μm. These distributions were similar for base–carbon and CNT–carbon composites at the source and breathing zone. The maximum particle number concentration at these peaks varied by composite type and particle size from 0.5–6.0E + 5 at 12 nm to 200–1,340 particles cm^{-3} at 1 μm. Trimming of baseline composite edges generated similar size distributions and TPNC as the CNT-containing composites themselves (Fig. 3A, B, #2; maximum number concentration 3.4E + 5 and 576 particles cm^{-3} at 12 nm and 1 μm, respectively), indicating that a large part of the generated aerosol resulted from fractionation of the base composite structure. The size distribution of base–alumina and CNT–alumina was slightly different than that of carbon-based composites. The second maximum for base–alumina composites (also the largest) was at 30 nm instead of 12, whereas for CNT–alumina was at 25 nm. Both alumina composites generated larger distributions in the 1–10 μm range than carbon-based composites. The particle number concentration for alumina composites at the source varied from 5.3E + 4 to 2.7E + 5 and 155–310 for the 25–30 nm and 1.1 μm, respectively. Size distributions in the 5.6–560 nm range of various composites at location 2 (Fig. 2B) were comparable to those of location 1, except that the maximum values were slightly higher. For example, base–carbon and CNT–carbon composites generated a maximum of 1.4E + 5 particles cm^{-3} at 12 nm, ~10,000 times higher than the corresponding background levels (~10–20 particles cm^{-3}). Base–alumina and CNT–alumina composites reached a maximum of 1.1E + 4 and 7.0E + 3 particles cm^{-3}, respectively.

Particle size distribution during wet cutting of base–carbon composites (Fig. 6C and C-1), unlike those from dry cutting of composites, was a broad monodisperse distribution with the maximum at 165 nm (spread 0.045–0.54 μm) and maximum value of 1.92E + 5 particles cm^{-3}. Concentration of particles >0.7 μm was <80 particles cm^{-3}.

Surface area

Surface area (SA) is a relevant exposure metric for nanoparticles and particulate matter and may also be a better metric than particle number concentration. Two reasons include: (i) biochemical and physical interactions of particles with biological systems are a surface phenomenon; (ii) surface area can be meaningfully summed up across a large particle size range, whereas particle number cannot. SA for particle number concentration measurements (location 1, Fig. 2B) presented in previous sections in four main fractions of interest are summarized in Tables 1 and 2: nano (≤100 nm size), fine (>0.1 to ≤1 μm); respirable (>1 to ≤10 μm) and thoracic (>10 to 20 μm). The mean total SA at the source varied from 1.3E + 3 (background) to 4.6E + 5 (base–carbon) μm^2 cm^{-3} in the following order: base–alumina 7.7E + 4, CNT–alumina 2.4E + 5, base–carbon 4.6E + 5, and CNT–carbon 3.9E + 5 μm^2 cm^{-3}. The mean total SA at the breathing zone was ~1.5–3.2 times lower than at the source, except for CNT–alumina, which generated a SA two times higher.

The wet cutting of base–carbon composites in the last test (June 12, 2008; broken guard—see Fig. 5 and associated discussion) produced a total SA of 1.2E + 5 μm^2 cm^{-3}; 3.8 times lower than its dry cutting equivalent. Although uncertain, it is likely that a large fraction of this aerosol is water.

The SA values for dry cutting of all composites varied by process and size fraction. The respirable fraction (1–10 μm) contributed 71–89% of the total SA followed by the fine (0.1–1 μm) fraction (6–25%). Contribution from the nano fraction (≤100 nm) was 1–10%, small compared to the respirable fraction. In contrast to dry cutting, the SA distribution for wet cutting was quite different; 85% of the total SA came from the fine fraction and 11% from the nano fraction. There are no significant differences in the SA fraction distributions between base- and CNT-composites.

Total dust concentration

In dry cutting, the mean PM_{10} dust mass concentration as measured by the TSI Dust-Trak™ for processes of Fig. 3 (location 1 in Fig. 2B), summarized in Tables 1 and 2, ranged from 0.013 (background) to 8.38 mg m^{-3} (CNT–carbon composites). Mean dust values for location 2 of Fig. 2B ranged from 0.041 (background) to 2.11 mg m^{-3} for CNT–carbon with intermediate values for other composites. It is interesting to note that mean dust values for location 2 were lower than for location 1, although the TPNC as measured by FMPS and CPC were higher in location 2.

The mean PM_{10} dust mass concentrations during wet cutting in all, but the June 12th tests were not

Table 2 Summary of airborne exposures *at the personal breathing zone* of the operator (associated with location 1 in Fig. 2B) as a function of composite parameters during dry cutting

Composite	Laminate specifications		AM (SEM) of total number concentration (# cm^{-3})		AM surface area (μm^2 cm^{-3}) by size range (its fraction of the total surface area)					Integrated sampling		
	No. plies	CNT fraction (# cm^{-3})	FMPS	APS	$d_p \leq 0.1$ μm	$0.1 < d_p \leq 1.0$ μm	$1 < d_p \leq 10$ μm	$10 < d_p \leq 20$ μm	$\sum$	RF (F cm^{-3})	R. dust (mg m^{-3})	AM PM_{10} dust (mg m^{-3})
Base–alumina	4	–	0.88E + 5 (0.51E + 4)	72.2 (4.6)	3,102 (0.13)	4,053 (0.16)	24,768 (0.71)	44 (0.00)	31,966 (1.0)	0.2	2.0	0.73
CNT–alumina	4	2.0 E + 12	0.28E + 5 (0.69E + 3)	62.2 (4.6)	711 (0.04)	10,517 (0.29)	33,374 (0.67)	54 (0.00)	44,656 (1.0)			0.80
Base–carbon	24	–	3.19E + 5 (1.12E + 4)	777.5 (26.1)	7,311 (0.03)	32,487 (0.12)	27,0961 (0.85)	1,769 (0.00)	312,528 (1.0)			5.41
CNT–carbon	24	1.5 E + 11	1.53E + 5 (0.77E + 4)	215.7 (11.5)	4,150 (0.05)	30,917 (0.34)	79,899 (0.61)	544 (0.00)	115,509 (1.0)			2.40

d_p, Aerodynamic diameter; AM, arithmetic mean; SEM, standard error of mean; FMPS, fast mobility particle sizer instrument; APS, aerodynamic particle sizer instrument; $\sum$, sum; RF, respirable fibers (length > 5–20 μm, aspect ratio >3) measured in fibers per cubic centimeter (F cm^{-3}). R. Dust, respirable dust from integrated sampling in micrograms m^{-3}; PM_{10}, particulate matter <10 μm (equivalent to respirable dust) measured by Dust Track, background corrected. All laminates 2.9-mm thick

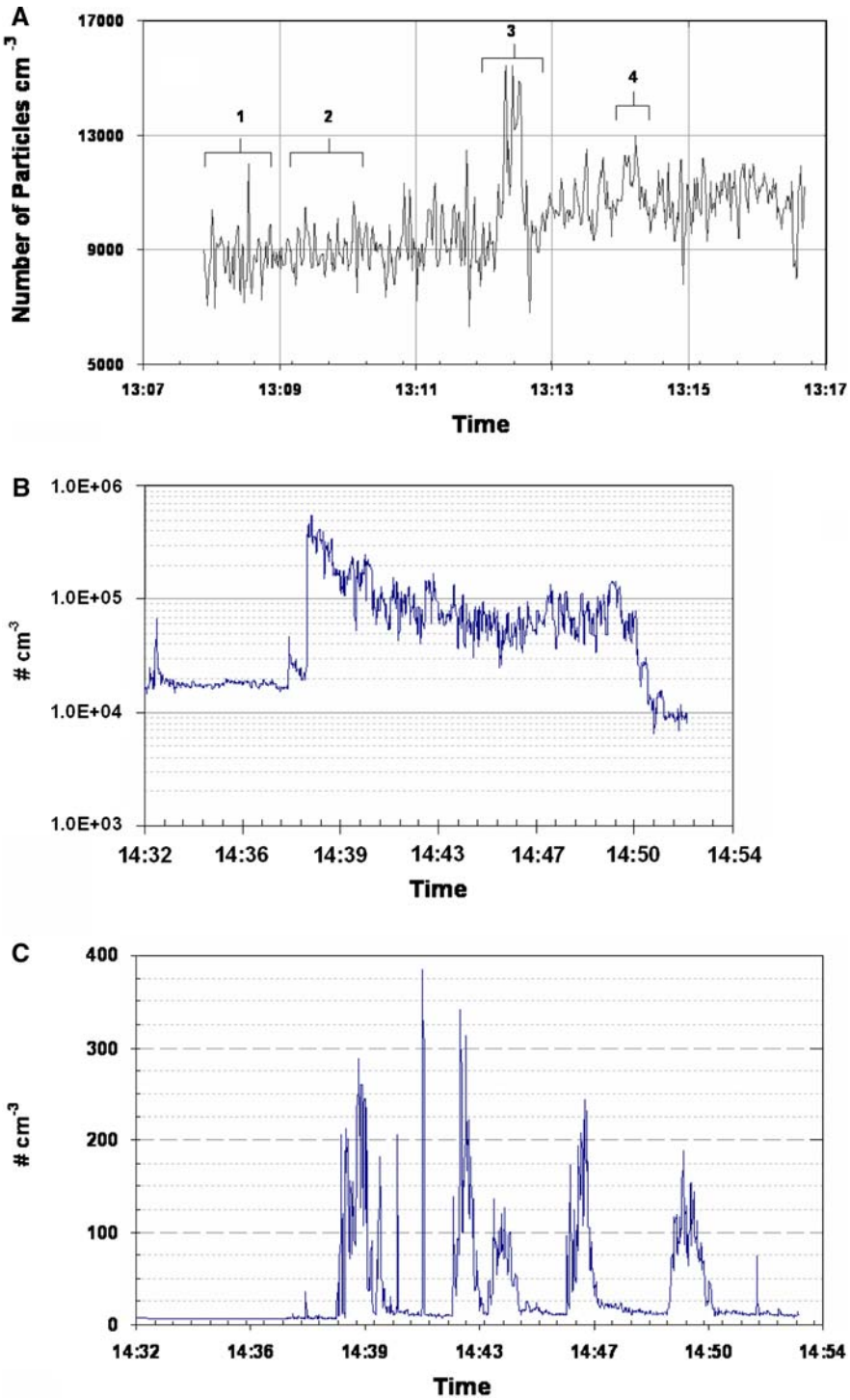

Fig. 5 Total particle number concentration during wet cutting: (**A**) FMPS total particle number concentration during wet cutting (July 31, 2007) showing no particle release [**A**-1. Background; 2 and 4. 24-ply baseline–carbon composite (without CNTs) under same conditions; 3. Same as in # 2, but the flow of water was intentionally reduced.] This profile was typical of all prior wet cutting tests (except the last one on June 12, 2008). (**B**) and (**C**) represent the total particle number concentration during the June 12, 2008 testing (damaged guard on cutting wheel) session for the FMPS (5.6–560 nm) and APS (<0.5–20 μm), respectively. The cluster of individual maxima on (**C**) represents individual tests on 24-ply base–carbon composites

statistically significant from background ($p > 0.05$) and commonly varied between 0.02 and 0.04 mg m^{-3}. The PM_{10} mean in the latest wet cutting tests was 0.054 mg m^{-3}, about four times higher than background, but ~10–100 times less than that in the dry cutting tests, confirming the focus of the most recent testing on dry cutting with no exposure controls.

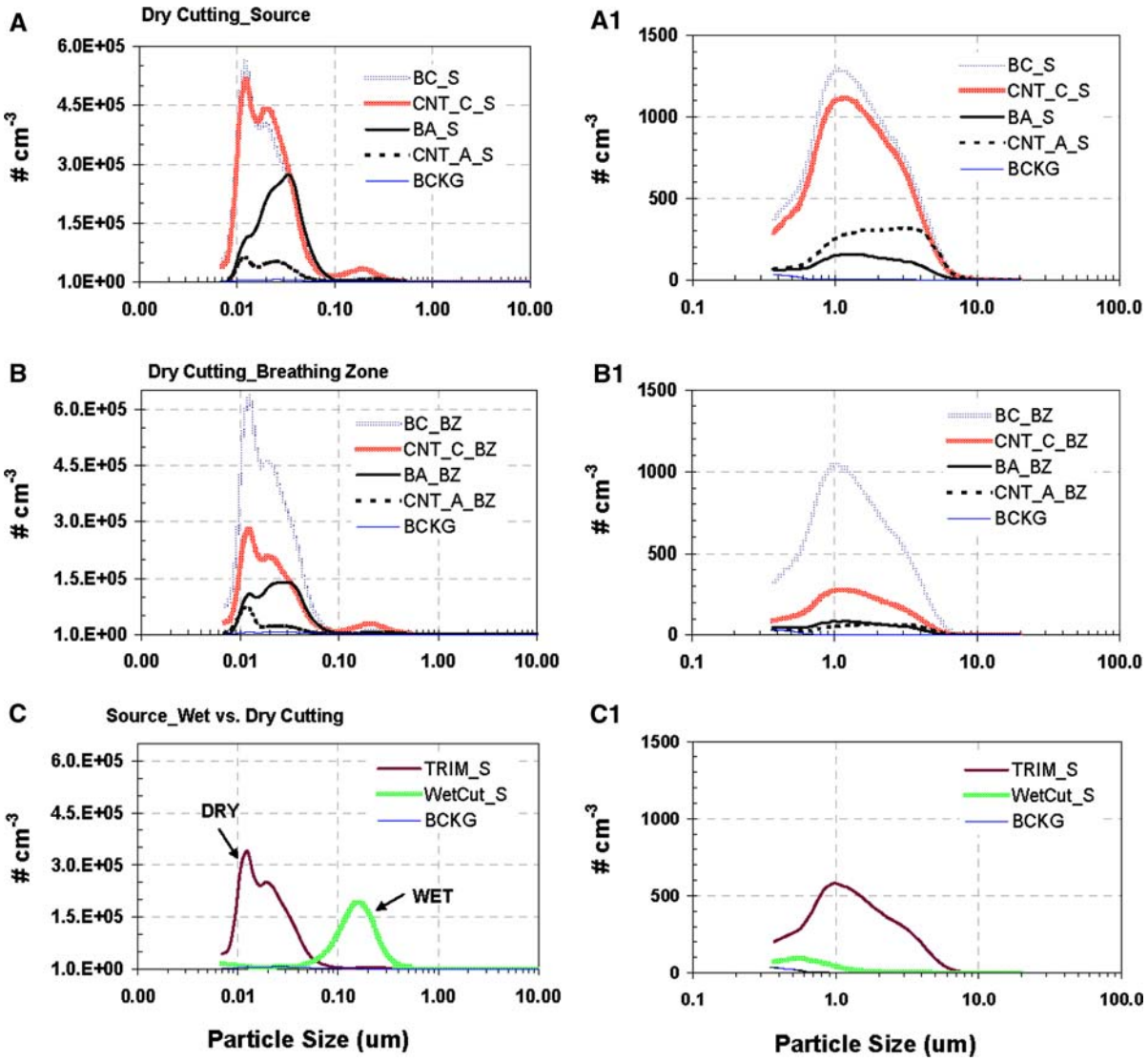

Fig. 6 Particle size distribution over the combined range 0.005–20 μm corresponding to Fig. 3A and B as measured by the FMPS and APS. Graphs **A**, **B**, and **C** represent combined FMPS and APS size distribution, whereas **A1**, **B1**, and **C1** are the APS portion of graphs (**A**–**C**). Lines are of arithmetic mean values of each channel. Standard errors of the mean (SEM) bars have been omitted for clarity purposes. The SEM varied between 2.5 and 5.9% of the mean. Legend: _S, at the source; _BZ, at the breathings zone; BC, base–carbon composite; CNT_C, CNT–carbon composite; BA, base–alumina composite; CNT_A, CNT–alumina composite; BCKG, background air; TRIM, trimming of composite edges; WetCut, wet cutting

Morphology of particles and fibers

Select representative images of particles collected during dry cutting of baseline and CNT–carbon and CNT–alumina composites are shown in Figs. 7 and 8. Nanoscale particles are best illustrated in images (D)–(F) of Fig. 7. Images of (A) and (B) of Fig. 7 are illustrative of typical low magnification field of TEM grids, whereas image (C) illustrates a respirable particle of very complex morphology, commonly observed during optical microscopy and SEM analysis of filters from dry cutting processes.

Representative images of the morphology of fibers is illustrated in Fig. 8. Images (A), (B) and (D) represent three common types of respirable fibers seen under PCM. Fibers originating from breakage of advanced

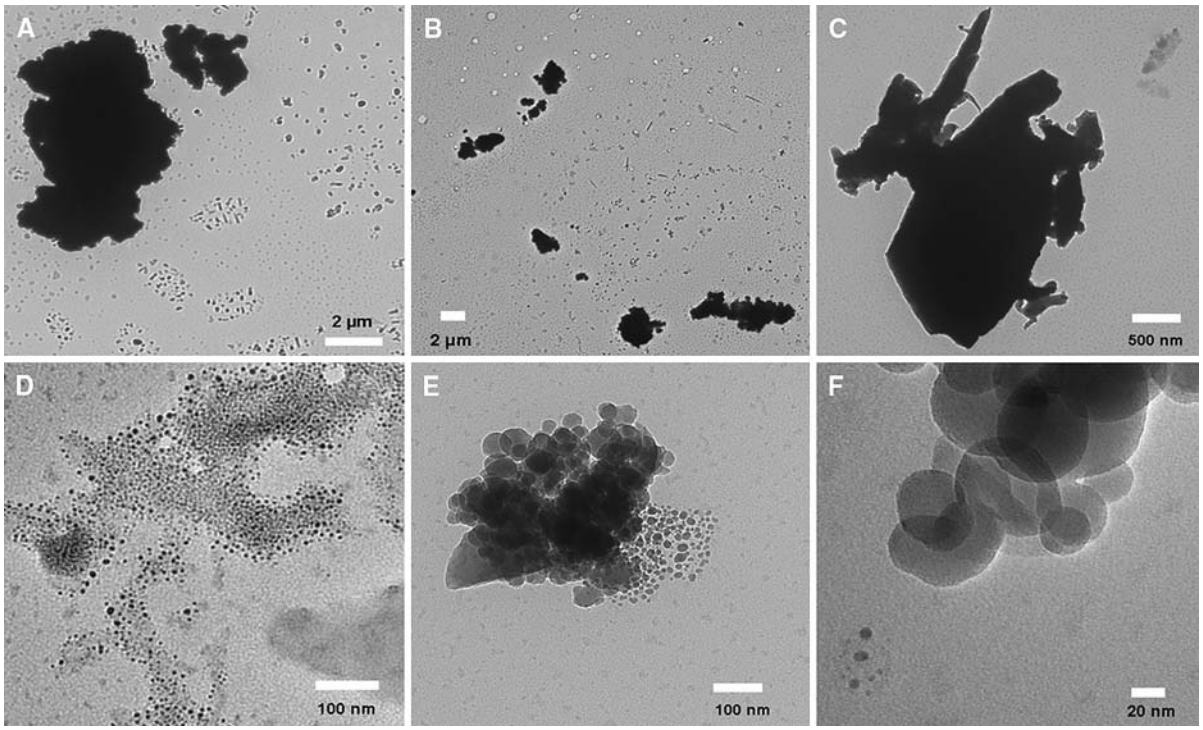

Fig. 7 Representative TEM images of samples collected during dry cutting of various composites illustrating: a wide range of particles (**A**, **B**); particles with very complex morphologies common to all composites (**C**); abundance of 10–20 nm particles on all composites; a typical enlargement of agglomerates and large particles such as those in image **B** (**F**). Images (**A**) and (**C**) originated from dry cutting of base–carbon composites, (**B**) from CNT–alumina composites, whereas (**D**–**F**) from CNT–carbon composites

fibers in the composites (base- and CNT-composites) perpendicular to their axis are shown in Fig. 7A for a carbon fiber. They are characterized by relatively smooth surfaces and typical fiber diameters >5 μm, resulting in smaller aspect ratios. The carbon fibers have nominal diameter of 6–7 μm, while the alumina fibers have a nominal diameter of 11 μm. Fibers of the type in image (B) may have originated from fracturing of advanced fibers along their axis, whereas those of images (D) and (E) may have originated from fracturing at or near the CNT–polymer interface layer. These types of fibers (B, D, E) are typically thinner, longer, and have higher aspect ratios than those associated with fractured advanced fibers.

Another common fiber type is depicted in images (C), (F), and (G) of Fig. 8. These submicron fibers typically have nanoscale diameters (5–20 nm) and have straight needle-like shapes. No clearly distinguishable contours of individual or bundles of CNTs could be found associated with any of the fibers and particle agglomerates, despite careful (>80 h) examination at maximum magnification of tens of fields from 15 TEM grids.

Respirable fibers, defined as having a length of >5–20 μm and an aspect ratio (length/width ratio) >3, are of the greatest toxicological interest, due to the fact that this fiber length is capable of causing lung cancers (such as mesothelioma from asbestos). Fibers shorter than ~1 μm in length are referred to as submicron fibers, whereas those longer than 30 μm are termed supramicron fibers. These latter fibers may be too large to enter the respiratory tract and are of lesser concern, whereas fibers <5 μm (including some submicron fibers) are expected to behave like particles in the lungs. Since the nanocomposites fabricated for this study also contain carbon (straight, collinear fibers) and alumina (woven) fibers, these will be referred to specifically as alumina and carbon advanced fibers, respectively. These advanced fibers commonly have a smooth, regular, cylindrical shape with a diameter of 5+ μm and length that exceeds meters (continuous advanced fibers, as opposed to short fibers commonly

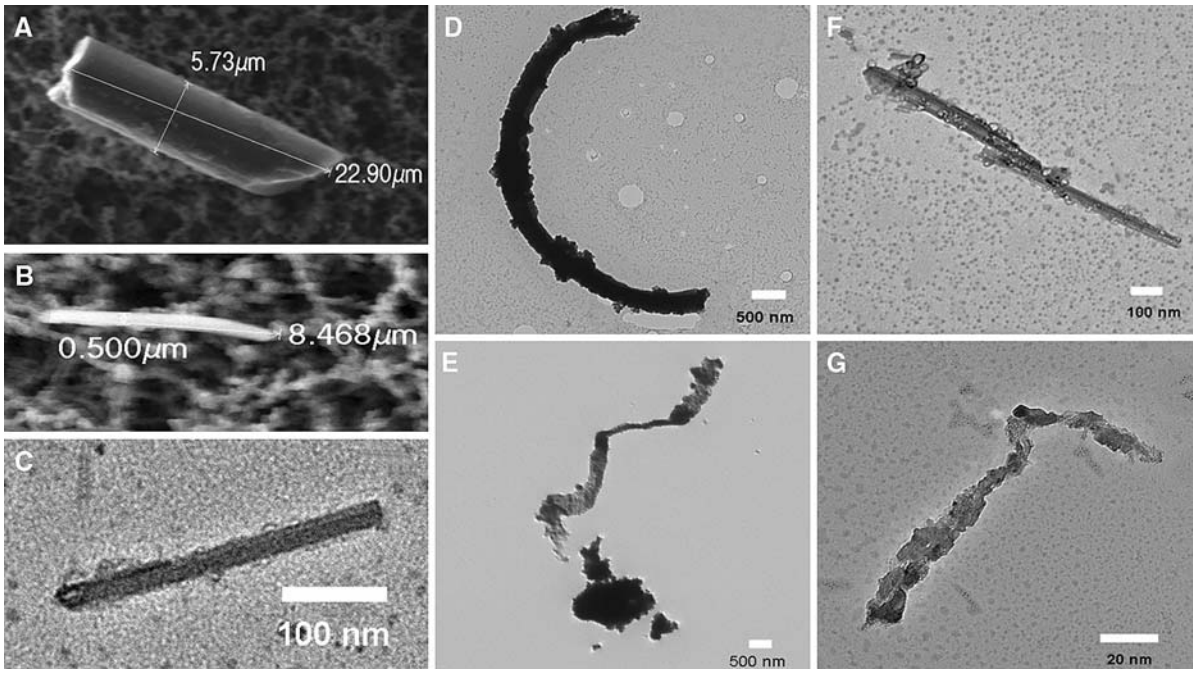

Fig. 8 Representative SEM and TEM images of fibers generated during dry cutting of various composites. (**A**) (SEM image) Depicting one common fiber type originating from fractionation of advanced fibers in composites; (**B**) (SEM image), (**D**), and (**E**) illustrate the morphology of the second most common respirable fiber type, whose origin may be splitting of advanced fibers or fracturing of the CNT–composite interface; (**C**), (**F**), and (**G**) represent common submicron fibers with at least one nanoscale dimension seen in all composites. No loose CNTs, either individual or bundles, were seen on maximum enlargement of these particles and respirable fibers. Images correspond to the following samples: (**A**) and (**B**)—integrated breathing zone filter from dry cutting (Fig. 4); (**C**, **F**, **G**)—CNT–alumina; (**D**), (**E**)—CNT–carbon

found in lower-quality composites such as sheet-molding compound).

Source and breathing zone concentration of respirable fibers for dry cutting are presented in Tables 1 and 2. Source concentration of respirable fibers was 1.6 fibers cm^{-3} for both alumina composites and 3.8 for base–carbon composites. A single filter collected during dry cutting of CNT–carbon composites at the source was lost due to an operator error. Breathing zone concentration of respirable fibers was 0.2 fibers cm^{-3} ($n = 2$). As per NIOSH method, a total of 100 graticule fields were examined by PCM for each filter. The total number of fibers per 100 graticule fields varied from 11 to 70, the fiber density was in the range of 14–89 fibers mm^{-2} and the sample volume 4–70 L. The method considers these parameters as less than optimal for accurate analysis and the results should be seen as an approximation.

The elemental composition of particles and fibers from the integrated EDS detector typically contained C, O, Fe, Co, Ni, Al, and Si. Al and Si were found only on TEM grids from cutting of base–alumina and CNT–alumina composites and were often accompanied by Fe and less frequently other elements such as Cr and Ca. Si was found in the alumina fiber itself. The alumina fiber has high alumina content, but also contains other refractory oxides including Si. Elements such as Co, Ni, and Cr may have also come from the grinding tool itself. Fe is used as a catalyst to facilitate the growth of CNTs for both CNT–alumina and CNT–carbon composites.

Discussion

This study investigated source and breathing zone exposures to airborne particles during dry and wet cutting of base alumina, CNT–alumina, base carbon, and CNT–carbon advanced composites. In dry cutting, none of the typical engineering control measures for reducing particle emission were implemented so that maximum source emissions could be assessed.

Special emphasis was put on characterization of nanoscale particles and respirable fibers and differences due to the presence of CNTs in composites.

This investigation produced several findings. Significant exposures to nanoscale particles compared to background were generated during dry cutting of all composites. Although these results are somewhat expected due to the nature of the process, dry cutting (particularly with no exposure controls) is generally not a preferred laboratory method for processing of advanced composites and, whenever used, requires effective engineering controls in place to control exposures. Breathing zone exposures were generally, but not always, lower than the source exposures. The particle size distributions of most composites were similar. Elemental composition of these particles matched reasonably well the expected composition of processed composites. Although the TPNC was dominated by the nanoscale and fine fractions, 71–89% of the total SA was dominated by the respirable (1–10 μm) aerosol fraction.

Submicron and respirable fibers were generated from dry cutting of all composites. The base–alumina and CNT–alumina composites generated about 1.6 respirable fibers cm^{-3}, ~2.4 times less than the base–carbon composites. No obvious differences were found in the behavior of base- and CNT-composites with regards to their tendency to generate respirable fibers and particles. Breathing zone concentration of respirable fibers (~0.2 fibers cm^{-3}) are still of concern in spite of these concentrations being an order of magnitude lower than source concentrations. Importantly, submicron long, thin (5–20 nm in diameter) and sharp, needle-like fibers were also found for all composites. Although they could not be quantified, such fibers were common. Fiber morphology and elemental composition suggest they may be originating from two distinct processes: fracturing of advanced fibers along their axis or perpendicular to it, and fracturing of the CNT composite at the interface. We are not aware of any other study reporting the findings of respirable and submicron fibers or characterization of nanoscale particle and fiber exposures during dry cutting of advanced CNT composites. A recent study reported potential exposure to CNT bundles during handling of the dry powder as part of nanocomposite (CNTs in epoxy) processing (Methner et al. 2007). Another recent study reported the release of considerable quantities of multiwalled CNTs (194 MWCNTs cm^{-3}) during their blending as part of a nanocomposite formulation process in a research laboratory setting (Han et al. 2008). Although these data are not comparable to our study because the processes are different, they illustrate the potential for release of MWCNTs.

No clearly identifiable individual CNT structures or bundles could be found in fibers or the particle agglomerates. This observation begs for an explanation as to why CNTs and CNT walls were not seen in TEM imaging of samples collected during processing of CNT-composites. Reasons may include epoxy encapsulation of CNTs, thick particles, and variable beam angle in regard to the CNT alignment inside the fibers and/or particles. Another explanation that needs further investigation may be that the CNTs in the polymer bind together so as to produce larger fibers and particles during cutting than resolved in this study (20 μm). Lack of resolution is not a likely explanation, as sufficient resolution down to 1 nm scale was routinely achieved. It is also unlikely that CNTs were missed during the TEM analysis given the extensive work (number of grids and the hours spent under TEM). One study has reported seeing MWCNTs sticking out of larger particles following mechanical sanding of a 1% MWCNT in a carbon–carbon composite in a glove box (Gupta et al. 2006). Detached individual CNTs were not reported in that study as well.

No striking differences in their tendency to generate particles and/or fibers during dry cutting were found between the base and its respective CNT-composite for both alumina and carbon composites (see Tables 1 and 2), with the exception of 1-ply CNT–alumina discussed below. It is conceivable that the tendency of a material to generate particles during cutting will be related to component adhesive properties, the number of plies in the composite, cutting tools and methods, as well as other factors. Indeed, the 24-ply (~2.9-mm thick) carbon composites generated significantly more exposure than the 4-ply (~2.9-mm thick) base–alumina composites. However, the investigative nature of this study and its focus on exposure characterization and not exposure determinants did not allow for complete standardization of these various parameters. Nevertheless, repeated tests with 1- and 2-ply base and CNT–alumina composites of identical thickness seems to support the hypothesis that the thickness (or number

of plies) of the composite is an important determinant of the tendency of these composites to generate airborne particles. Four-ply (~2.9-mm thick) base–alumina composites generated slightly more exposure than the 1- to 3-ply base–alumina composites. The thinnest specimen (1-ply CNT–alumina composite, 0.6-mm thick) always generated the least nanoscale particle number concentration. Overall, the CNTs in thin composites of a few layers reduced airborne exposures, whereas for thick composites there was no such effect.

Wet cutting in all, but one test (broken guard) reduced exposures to background levels. In one test, during which the guard around the rotary wheel was visibly damaged, wet cutting generated significant airborne exposures compared to background. Although airborne particulate matter was clearly emitted during this test (as confirmed by deposition of black aerosol on surfaces) and the size distribution was distinct from dry cutting (monodisperse, maximum at 200 nm), it is unclear how much of that aerosol was water. Concerns over instrumentation damage in the presence of high water aerosol concentrations discouraged us from further tests. The normal practice at this laboratory is that the machine should not be operated with a worn guard. Similarly, Methner et al. (2007) reported 1.1 mg total carbon m^{-3} inhalable aerosol collected with integrated sampling during wet cutting of CNFs (carbon nano fibers, not nanotubes). Although these data cannot be compared to ours, their finding of possible emissions during wet cutting is consistent with one of our observations. Wet cutting was an efficient processing and control method only when the protective guard of the rotary wheel was intact. In regards to inhalation exposures, wet cutting is likely a superior post-processing method for advanced and hybrid composites compared to dry cutting, and is the preferred method in use at the present time at the laboratory where this research was conducted.

Last, it should be remembered that dry cutting without emission controls leading to high exposures in this study were very short (<1 min) and occurred infrequently. Exposures themselves were mostly to fine particulates and respirable and submicron fibers. Hence, averaged over an 8-h shift these exposures, especially with the use of a respirator and additional engineering controls, exposures will be much lower. Nevertheless, generation of respirable fibers in concentrations >0.1 fibers cm^{-3} is particularly of great concern given potential carcinogenicity associated with such fibers. At present it is not possible to quantitate the health risks associated with the measured nanoscale particles or fibers and it is prudent to continue to exercise care to minimize inhalation exposures.

As to dust exposures during dry cutting with no emission controls, there are 8-h Threshold Limit Values (TLV, ACGIH 2007) for poorly soluble respirable particles and graphite of 3, and 2 mg m^{-3}, respectively. One integrated (454 L, 108 min) respirable breathing zone sample resulted in an average of 2.0 mg m^{-3} dust, which is within the range of average dust concentrations measured by the dust track. Averaged over an 8-h period, such intermittent exposures will be over an order of magnitude lower than the TLV. However, total dust and fine particle exposures may be of greater concern in other scenarios, such as during manufacturing scale up, longer and more sustained operations, or lack of controls. Furthermore, these TLVs do not reflect exposure to nanoscale particles.

The question of biological significance of exposures to nanoscale particles and fibers as observed in this study is of special interest and beyond the scope of this article. Interested readers may find the review by Donaldson et al. (2006) beneficial. Important properties for toxicity of fibers, such as their length (>5–20 μm, or nanoscale <100 nm dimensions), biopersistence, presence of transition metal contaminants (especially Fe, Cr, and Ni) and organic impurities, and the large surface area associated with the fine particulate fraction, are all factors known to increase toxicity of particulate matter and fibers, further emphasizing the necessity of exposure prevention and continued research into toxicity of such exposures.

Study limitations

This study employed a tiered approach and multiple instrumentations to characterize exposures to nanoscale and respirable fibers during dry cutting of advanced composites with and without CNTs. In this approach, early testing findings were utilized to improve the design and modify the research objectives in subsequent visits. Repeat visits, multiple complementary instrumentations, characterization of

the components of size distribution of particles at the source and the breathing zone, quantitation of respirable fibers, and extensive electron microscopy are characteristics of this study. However, this study also has some limitations. First, fabrication of advanced composites was time consuming and evolved over the course of the study, and cutting was a destructive processing method. This restricted the number of paired tests performed on available specimens at any given time. Second, protocols showed some variability between visits, in part because select expensive instruments were not available for some tests, and they were modified in response to new findings. Third, airborne concentration of submicron fibers, which were numerous under TEM, could not be quantitated. Fourth, wet cutting was incompletely characterized in the last visit because all prior tests were negative and concerns over instruments damage from water restricted testing. Exposures during wet cutting require further investigation, in order to separate water aerosol from particulate matter and to confirm size distribution and morphology of particles as was done with dry cutting. Fifth, no quantitative analysis for transition metals (Fe, Cr, Co, and Ni) using sensitive analytical techniques such as ICP-MS (inductively coupled plasma-mass spectrometry) could be performed. Lastly, this study was focused on characterization of exposures, but not controls or exposure determinants. Further studies investigating these factors are needed and underway.

Conclusions

Dry cutting of base- and CNT-containing composites without emissions controls resulted in high airborne exposures to nanoscale and fine particles as well as submicron and respirable fibers. Exposure levels were dependent on composite thickness and type, but overall particulate levels as well as concentrations of nanoscale and fine particles and fibers did not vary between composites with and without CNTs. No evidence of individual CNTs, bundles of CNTs, or CNTs attached to larger particles were observed for all composites. The toxicological profile of airborne nanoscale and fine particles and fibers generated during dry cutting of advanced CNT composites is not well known, but concerning nonetheless and great care should be exercised to avoid or control such exposures. Wet cutting, under optimal operational conditions, is a superior post-processing method compared to dry cutting. Further investigations are needed to understand various exposure determinants, such as tool geometry and composite properties, and to evaluate efficiency of various controls.

Acknowledgments This work was supported under the Nanoscale Science and Engineering Centers Program of the National Science Foundation (Award # NSF-0425826) and by Airbus S.A.S., Boeing, Embraer, Lockheed Martin, Saab AB, Spirit AeroSystems, and Textron Inc. through MIT's Nano-engineered composite aerospace structures (NECST) Consortium. Namiko Yamamoto acknowledges support from the Linda and Richard (1958) Hardy Fellowship. Authors would like to thank Dr. Arthur Miller of NIOSH for his generous offering of the prototype electrostatic precipitator and C. Santeufemio and Dr. Earl Ada of the UML Materials Characterization Lab for their technical assistance with EM analysis.

References

ACGIH (2007) 2007 TLVs® and BEIs®: threshold limit values for chemical substances and physical agents and biological exposure indices. American conference of governmental industrial hygienists, Cincinnati, OH. ISBN: 1-882417-62-3

Ajayan PM, Tour JM (2007) Materials science: nanotube composites. Nature 447(7148):1066–1068. doi:10.1038/4471066a

Ajayan PM, Schadler LS, Braun PV (2003) Nanocomposite science & technology, 1st edn. Wiley-VCH, Weinheim

Barlow PG, Clouter-Baker A, Donaldson K, Maccallum J, Stone V (2005a) Carbon black nanoparticles induce type II epithelial cells to release chemotaxins for alveolar macrophages. Part Fibre Toxicol 2:11. doi:10.1186/1743-8977-2-11

Barlow PG, Donaldson K, MacCallum J, Clouter A, Stone V (2005b) Serum exposed to nanoparticle carbon black displays increased potential to induce macrophage migration. Toxicol Lett 155(3):397–401. doi:10.1016/j.toxlet.2004.11.006

Bello D, Hart AJ, Ahn K, Hallock M, Yamamoto N, Garcia EJ et al (2008) Particle exposure levels during CVD growth and subsequent handling of vertically-aligned carbon nanotube films. Carbon 46:974–981. doi:10.1016/j.carbon.2008.03.003

Coleman JN, Khan U, Blau WJ, Gun'ko YK (2006) Small but strong: a review of the mechanical properties of carbon nanotube-polymer composites. Carbon 44:1624–1652. doi:10.1016/j.carbon.2006.02.038

Donaldson K, Aitken R, Tran L, Stone V, Duffin R, Forrest G et al (2006) Carbon nanotubes: a review of their properties in relation to pulmonary toxicology and workplace safety. Toxicol Sci 92(1):5–22. doi:10.1093/toxsci/kfj130

Foucaud L, Wilson MR, Brown DM, Stone V (2007) Measurement of reactive species production by nanoparticles prepared in biologically relevant media. Toxicol Lett 174(1–3):1–9. doi:10.1016/j.toxlet.2007.08.001

Garcia EJ, Hart AJ, Wardle BW, Slocum AH (2007) Fabrication of composite microstructures by capillarity-driven wetting of aligned carbon nanotubes with polymers. Nanotechnology 18(16):165602. doi:10.1088/0957-4484/1018/1016/165602

Garcia EJ, Wardle BL, Hart AJ, Yamamoto N (2008a) Fabrication and multifunctional properties of a hybrid laminate with aligned carbon nanotubes grown in situ. Compos Sci Technol 68(9):2034–2041. doi:10.1016/j.compscitech.2008.02.028

Garcia EJ, Wardle BL, Hart AJ (2008b) Joining prepreg composite interfaces with aligned carbon nanotubes. Composites Part A 39:1065–1070. doi:10.1016/j.compositesa.2008.03.011

Gupta A, Gaspar DJ, Yost MG, Gross GM, Rempes PE, Clark ML et al (2006) Evaluating the potential for release of carbon nanotubes and subsequent occupational exposure during processing of a nanocomposite. In: Nanotechnology occupational and environmental health and safety 2006, Cincinnati, OH

Han JH, Lee EJ, Lee JH, So KP, Lee YH, Bae GN et al (2008) Monitoring multiwalled carbon nanotube exposure in carbon nanotube research facility. Inhal Toxicol 20(8):741–749. doi:10.1080/08958370801942238

Hart AJ, Slocum AH (2006) Rapid growth and flow-mediated nucleation of millimeter-scale aligned carbon nanotube structures from a thin film catalyst (with cover). J Phys Chem B 110:8250–8257. doi:10.1021/jp055498b

Lam CW, James JT, McCluskey R, Hunter RL (2004) Pulmonary toxicity of single-wall carbon nanotubes in mice 7 and 90 days after intratracheal instillation. Toxicol Sci 77(1):126–134. doi:10.1093/toxsci/kfg243

Lam CW, James JT, McCluskey R, Arepalli S, Hunter RL (2006) A review of carbon nanotube toxicity and assessment of potential occupational and environmental health risks. Crit Rev Toxicol 36(3):189–217. doi:10.1080/10408440600570233

Lavine M (2006) The right combination. Science 314:1099. doi:10.1126/science.314.5802.1099

Methner MM, Birch ME, Evans DE, Ku BK, Crouch K, Hoover MD (2007) Identification and characterization of potential sources of worker exposure to carbon nanofibers during polymer composite laboratory operations. J Occup Environ Hyg 4(12):D125–D130. doi:10.1080/15459620701683871

Poland CA, Duffin R, Kinloch I, Maynard A, Wallace WAH, Seaton A et al (2008) Carbon nanotubes introduced into the abdominal cavity of mice show asbestos-like pathogenicity in a pilot study. Nat Nanotechnol 3:423–428. doi:10.1038/nnano.2008.111

Rogers E, Hsieh SF, Rao N, Schmidt D, Bello D (2008) A high throughput analytical approach to screen for oxidative stress potential exerted by nanomaterials in a biologically relevant matrix: human blood serum. Toxicol In Vitro 22:1639–1647. doi:10.1016/j.tiv.2008.06.001

Schulte K, Windle AH (2007) Carbon nanotube (CNT)–polymer composites. Comp Sci Tech 67(777):Entire issue

Shvedova AA, Kisin ER, Mercer R, Murray AR, Johnson VJ, Potapovich AI et al (2005) Unusual inflammatory and fibrogenic pulmonary responses to single-walled carbon nanotubes in mice. Am J Physiol Lung Cell Mol Physiol 289(5):L698–L708. doi:10.1152/ajplung.00084.2005

Thostenson ET, Li C, Chou W (2005) Nanocomposites in context. Comp Sci Tech 65:491–516. doi:10.1016/j.compscitech.2004.11.003